IEEE Access
Multidisciplinary | Rapid Review | Open Access Journal

Received September 3, 2020, accepted September 26, 2020, date of publication September 30, 2020,
date of current version October 9, 2020.

Digital Object Identifier 10.1109/ACCESS.2020.3027869

DC Series Arc Fault Detection Algorithm for Distributed Energy Resources Using Arc Fault Impedance Modeling

HWA-PYEONG PARK, (Member, IEEE), AND SUYONG CHAE, (Member, IEEE)
Korea Institute of Energy Research (KIER), Daejeon 34129, South Korea

Corresponding author: Suyong Chae (sychae@kier.re.kr)

This work was supported by the Research and Development Program of the Korea Institute of Energy Research under Grant C0-2411.

ABSTRACT Arc fault detection is important technology to guarantee the safety of power systems and is therefore essential for producing practical power systems for real-world applications. However, fuses and arc fault detection devices (AFDD) struggle to detect series arc faults in DC systems, because the series arc fault induces small current variation between the normal and abnormal conditions. In addition, switching noise from the grid-connected inverter makes detecting arc fault conditions even more difficult. This paper proposes arc fault detection algorithm based on the relative comparison of current variability in terms of frequency spectrum and time series. The operational principle of the proposed algorithm is analyzed to detect the arc fault condition. In addition, the investigation of arc fault impedance using the small-signal modeling can obtain the resonant frequency of arc fault condition at low frequency range. From the impedance model, the frequency analysis range can be designed to avoid the switching noise of inverter. The performance of proposed arc fault detection algorithm is verified with a 3.8 kW grid-connected PV system and arc fault generator.

INDEX TERMS Arc fault, fault diagnosis, dc-ac inverter, digital signal processor.

I. INTRODUCTION

The conventional grid system was developed based on power generation from fossil fuels, which is primary source of environmental pollution. This has spurred interest and investment in renewable energy sources (RES), such as photovoltaics (PV) and wind power, which are strong candidates for obtaining clean energy [1]–[3]. In addition, the energy storage system (ESS) can be one of candidates to improve the energy efficiency [4]–[6]. Consequently, grid-connected RES have grown drastically in recent years, which are increasingly applied to the households and power distribution [7]–[9]. In addition, the interest in the safety of PV, ESS and its grid-connected inverters is increasing. Specially, PVs and ESS inherently handle a DC power, which can result in DC arc faults between the PV and inverter. Fig. 1 shows the DC series arc fault in the grid-connected PV and ESS systems. The National Electrical Code (NEC) therefore requires arc fault circuit interrupter (AFCI) installation in all PV DC systems over 80 V to ensure the safe use of this RES.

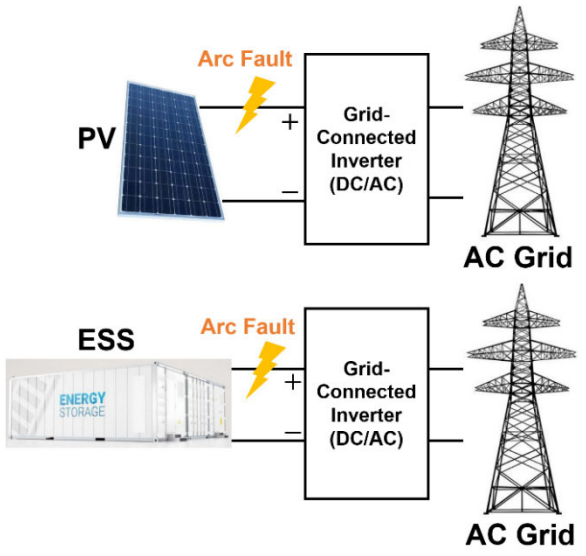

FIGURE 1. Structure of grid connected PV and ESS systems.

Two types of arc faults, parallel and series, can occur in DC systems [10], [11]. Parallel arc fault can be easily detected

The associate editor coordinating the review of this manuscript and approving it for publication was Manoj Datta.

by the large amount of current. However, detecting series arc faults is difficult as only a small current change occurs, which is not sufficient to melt fuses [12]. In addition, it makes hard to detect the arc fault in the time domain. Furthermore, the switching noise of inverter is dominant compared with the noise caused by the arc fault, which makes arc fault detection even more difficult in the frequency domain [13].

In previous research, several algorithms have been invented to detect DC series arc fault condition. In [10], [14]–[16], time domain analysis was introduced to detect the arc fault condition, which uses current and voltage information. These methods provide fast detection speeds with simple circuits and algorithms, but they are susceptible to switching noise and load variation. In [17] and [18], frequency analysis was applied to detect the arc fault condition, which is based on the fast Fourier transform (FFT) or short time Fourier transform. They extracted the features of arc fault condition compared with the normal operation in the frequency domain. In [19]–[21], the discrete wavelet transform (DWT) and wavelet packet transform (DPT) ware also introduced to detect the arc fault condition in the frequency domain. This method decomposes the frequency response to improve the resolution under the desired frequency range, which can magnify the noise signal caused by the arc fault condition. The previous research shows the multi-resolution analysis with their adjustable window functions. However, the arc fault detection performance using the frequency domain analysis depends on the frequency bandwidth selection. The conventional detection range is several tens kilo-hertz, which can degrade the detection accuracy by the switching noise of the inverter [17]–[21]. In [22], [23], the artificial neural network and support vector machines were introduced to detect the arc fault condition. In addition, the traditional machine learning, such as decision tree and fuzzy interference system, were introduced to detect the arc fault condition. The arc fault detection method based on the artificial intelligence uses various information for detecting fault conditions. The safety issue requires high reliability for the fault detection device. However, these methods have uncertainty about detection failure, which should be improved in the future.

In this paper, the arc fault detection algorithm is proposed using the statistical analysis of arc current variability in terms of time and frequency domains. The time domain analysis uses the standard deviation of current variation according to the arc fault condition, which cannot detect the arc fault condition solely. The frequency domain analysis using the fast Fourier transform (FFT) compares the relative magnitude variation according to the arc fault and no arc fault conditions. This paper also proposes the impedance model of arc fault condition under the low frequency range using the small signal modeling. From the analyzed impedance model, the frequency spectrum range of FFT can be designed to detect the arc fault condition and avoid the switching noise of inverter. The operational principle of the proposed algorithm and arc fault impedance model are analyzed in Section II and Section III. The performance of the proposed algorithm is verified with a 3.5 kW PV systems in Section IV.

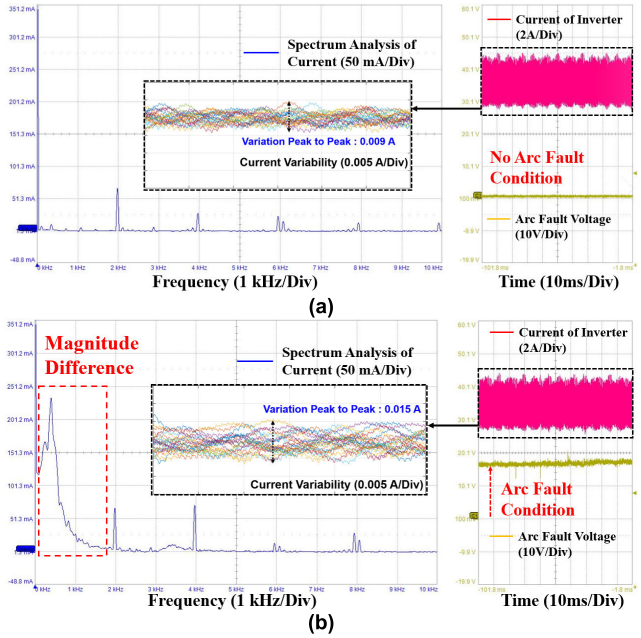

FIGURE 2. Frequency spectrum of PV DC current: (a) Normal condition and (b) Arc fault condition.

II. IMPEDANCE ANALYSIS OF ARC FAULT

The DC and AC characteristics of arc fault condition were analyzed in [25]. The previous impedance model presents the DC and AC characteristics with negative resistance and inductance. However, it cannot describe the AC characteristics of arc fault condition under the low frequency range. Fig. 2 (a) presents the base frequency spectrum of PV input current at the no arc fault condition. Fig. 2 (b) presents the frequency spectrum at arc fault condition. The arc fault condition increases variability of PV input current compared with normal condition. In addition, FFT results of arc fault condition has large magnitude variation at the low frequency range compared with the normal condition. This frequency range can avoid the switching noise of grid-connected inverter. This magnitude difference is amplified at the low frequency range with the variability of arc fault current and its resonant impedance.

Fig. 3 shows the transient operation according to the arc fault condition and resistance insertion. Fig. 3 (a) and (b) presents the schematic of resistance insertion and the transient operation using the circuit breaker. This test-bed system can simulate the arc fault condition with the resistance insertion in the DC power line. The on-state and off-state of circuit breaker shows the normal and abnormal conditions, respectively. However, it presents no resonance at the transient duration in the PV input current. Also, the line impedance of designed system does not induce the resonance in the PV current. Fig. 3 (c) and (d) shows the schematic of arc fault condition and the transient operation using the arc fault

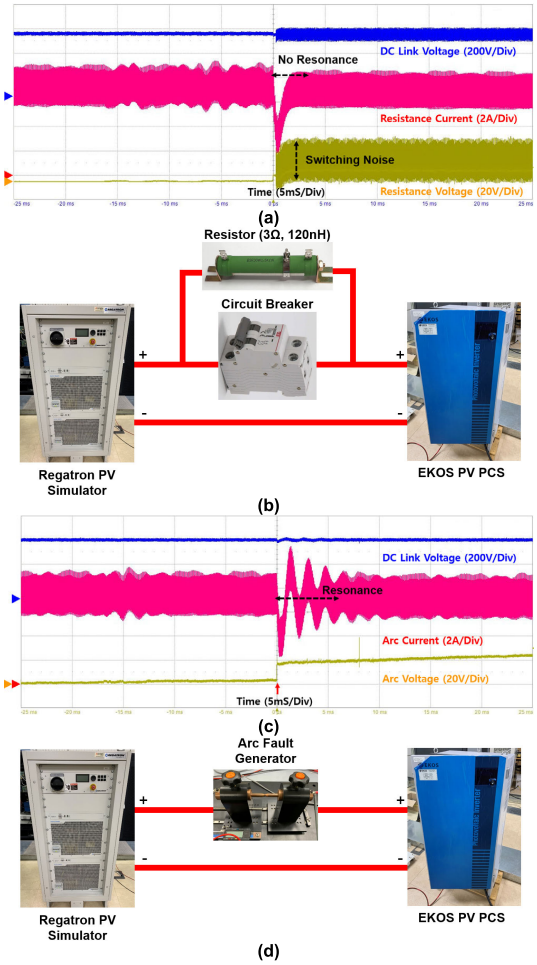

FIGURE 3. Abnormal operation and dynamic response: (a) experimental results of resistance insertion, (b) test-bed for resistance insertion, (c) experimental results of arc fault condition, and (d) test-bed system of arc fault condition.

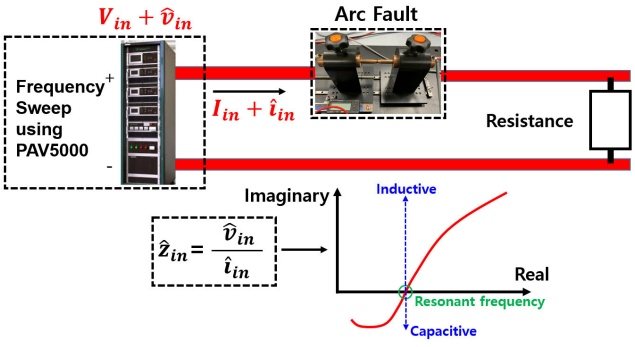

FIGURE 4. Experimental setup for gain-phase analysis.

generator. The designed test-bed system shows low frequency response in the PV input current according to the arc fault condition. From Fig. 3, the previous arc fault model using the series connected resistance and inductance cannot describe the low frequency AC characteristics of arc fault condition. Therefore, arc impedance must be improved to obtain suitable arc fault characteristics.

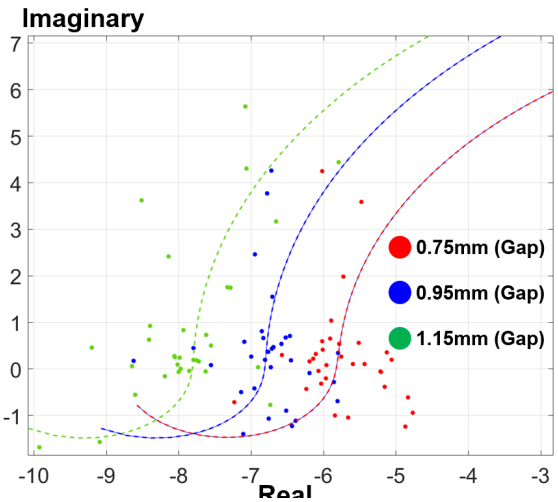

FIGURE 5. Nyquist plot of arc fault condition.

The gain-phase analysis via frequency sweep can obtain the impedance model of arc fault condition at the low frequency range. Fig. 4 shows the linear amplifier (PAV5000, PONOVO), non-inductive resistance, and arc fault generator. The linear amplifier can generate DC and AC coupled voltage and vary the frequency from DC to 5 kHz. It is proper to measure the impedance characteristics at the low frequency range (< 5kHz). The resistor has non-inductive components (20 Ω and 1.4 nH). The designed arc fault generator satisfies the UL 1699B standard. The oscilloscope (Teledyne Lecroy, Wavesurfer 4104HD) measures the voltage and current values, which can guarantee data precision with 500 MS/s. The impedance according to the normal condition and arc fault condition can be obtained, as follows:

$$Z_{tot,nor} = Z_{in} + Z_{load} \tag{1}$$

$$Z_{tot,arc} = Z_{in} + Z_{load} + Z_{arc} \tag{2}$$

where Z_{in} is the source impedance, Z_{load} is the load impedance, $Z_{tot,nor}$ is the total impedance at normal condition, and $Z_{tot,arc}$ is the total impedance at the arc fault condition. From (1) and (2), the arc fault impedance can be measured, as follows:

$$Z_{arc} = Z_{tot,arc} - Z_{tot,nor} \tag{3}$$

Fig. 5 shows the Nyquist plot using (3). The dots represent experimental arc impedances. Notably, it has capacitance and inductance at low frequencies. The chaotic variation of arc fault resistance induces current variation, which is amplified at the resonant frequency of arc fault as shown in Fig. 2 (b). In addition, the increase of rod gap and decrease of input voltage increase the negative resistance, inductance, and capacitance.

From the above Nyquist plot, the proposed arc impedance can be estimated, as shown in Fig. 6. The dashed lines in Fig. 5 show the theoretical arc impedance, and the DC negative resistance is shown at the resonant frequency (f_{res}) of

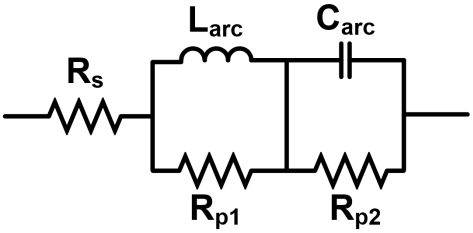

FIGURE 6. Arc impedance model at low frequency range.

C_{arc} and L_{arc}, which can be described as follows:

$$Z(f_{res}) \cong R_s \tag{4}$$

The capacitive and inductive impedances are calculated at the minimum and maximum frequencies (f_{min} and f_{max}) of AC sweep, respectively. The theoretical impedance at the

minimum and maximum frequency can be described as follows:

$$Z(f_{\min}) \cong R_s + \frac{R_{p2}}{j\omega C_{arc} R_{p2} + 1} \tag{5}$$

$$Z(f_{\max}) \cong R_s + \frac{j\omega L_{arc} R_{p1}}{j\omega L_{arc} + R_{p1}} \tag{6}$$

In addition, the resonant frequency of arc fault impedance can be derived, as follows:

$$f_{res} \cong \frac{1}{2\pi\sqrt{L_{arc} C_{arc}}} \tag{7}$$

The resonant frequency of arc fault impedance is located in the several kilo-hertz, which is lower than the switching frequency of grid-connected inverter. The arc fault detection near (7) can improve the reliability of designed detection algorithm.

III. ARC FAULT DETECTION ALGORITHM

The detection algorithm proposed here uses the arc current variability. The preprocessing circuit extracts the AC components of arc current and has low pass filter to cut off the switching noises. The controller obtains the current information from the preprocessing circuit, and the proposed detection algorithm uses the standard deviation of arc current in terms of the time series and frequency spectrum. Arc fault detection systems must distinguish arc fault condition from step load response and should detect small arc energies at the light load condition.

In the time domain, the moving average standard deviation of current can be derived as follows:

$$\sigma_i[n] = \sqrt{\frac{1}{M} \sum_{k=n-M+1}^{n} \left(i_{arc}[k] - i_{arc,aver}[n]\right)^2} \tag{8}$$

where σ_i is the standard deviation, M is the data samples, i_{arc} is the instantaneous arc current, and $i_{arc,aver}$ is the moving average of arc current. The abnormal condition of time series

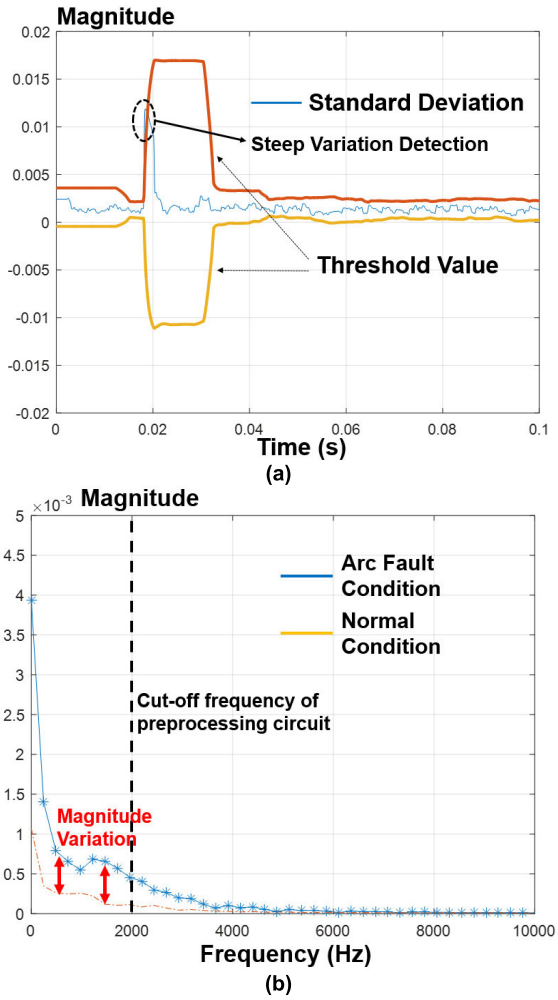

FIGURE 7. Arc fault detection: (a) Current variation using standard deviation, and (b) FFT standard deviation.

can be detected with the threshold value, which is designed with x-th sigma rules as follows:

$$\sigma_{th}[n] = \sigma_{aver}[n] + \alpha_{th}\sigma_{std}[n] \tag{9}$$

where σ_{th} is the threshold value, σ_{aver} is the moving average of σ_i, α_{th} is the threshold gain, and α_{std} is the standard deviation of σ_i. When the standard deviation is greater than the threshold value, the steep current variation caused by arc fault is detected, as shown in Fig. 7 (a). It presents the magnitude difference between normal and abnormal conditions. In addition, the threshold gain can be designed according to the desired precision of abnormal condition. For example, when the α_{th} is three, (8) and (9) has 99.7 % detection precision of abnormal condition. However, the time domain analysis using steep variation detection cannot distinguish the arc fault condition and load or power variation.

In the frequency domain, the FFT calculates the magnitude of arc current with the designed frequency bandwidth. The Fast Fourier Transform (FFT) analysis can be used to detect the arc fault condition by utilizing a fast computation speed

to calculate the Digital Fourier Transform (DFT). The DFT of PV DC current can be derived as follows:

$$I_{PV}[k] = \frac{1}{N}\left|\sum_{k=0}^{N-1} i_{PV}[n]\, e^{-j2\pi kn/N}\right| \tag{10}$$

where $I_{PV}[k]$ is the PV DC current according to the frequency analysis, k is the frequency bin, n is the number of sampling point, which can range from 0 to N. The frequency resolution is determined using the sampling frequency ($f_{sampling}$) and N and can be expressed as $f_{sampling}/N$. The number of complex DFT frequency components is defined as $N/2$.

In this experiment, the sampling frequency is 250 kHz and N is 1024. The designed FFT has 512 frequency bins with a 244.14 Hz frequency resolution. The standard deviation of FFT magnitude can be derived, as follows:

$$\sigma_f[u] = \sqrt{\frac{1}{P}\sum_{q=1-P}^{0}\left(I_{PV}[k,\, q] - \mu_{PV,freq}[k]\right)^2} \tag{11}$$

where σ_f is the standard deviation in the frequency domain, P is the number of FFT implementation, I_{PV} is the FFT magnitude of arc current, and $\mu_{PV,freq}$ is the moving average of the FFT magnitude. In this experiment, 20 times FFT are calculated to obtain (11), which induces 81.92 ms computation time. The relative comparison of standard deviation using (11) can distinguish the normal and arc fault condition. Fig. 7 (b) shows the standard deviation before and after the arc fault condition. The arc fault condition has higher magnitude compared with the normal condition under 4 kHz, which can overcome the switching noise of inverter. The arc fault condition shows high variability compared with the no arc fault condition at the low frequency range, which is also shown in Fig. 2.

The frequency spectrum range can be designed with the arc fault impedance, which can overcome the inverter switching noise. The resonant frequency of arc fault and its quality factor (Q) can be described, as follows:

$$f_{res} \cong \frac{1}{2\pi\sqrt{L_{arc}C_{arc}}}, \quad Q = \frac{\sqrt{L_{arc}/C_{arc}}}{R_{load}+R_{arc}}, \quad \Delta f_{arc} = f_{arc}/Q \tag{12}$$

where R_{load} is the load resistance of inverter, R_{arc} is the arc resistance, and Δf_{arc} is the resonant width. From (12), the theoretical FFT range to calculate the relative comparison can be derived, as follows:

$$f_{\min} = f_{arc} - \Delta f_{arc}, \quad f_{\max} = f_{arc} + \Delta f_{arc} \tag{13}$$

The arc resonant frequency is 450 Hz. The theoretical FFT frequency range of f_{min} and f_{max} is calculated as 150 Hz and 750 Hz, respectively. In this experiment, the designed FFT range is 100 Hz to 2 kHz to calculate the relative magnitude comparison, which is 10 times lower than the switching frequency of 25 kHz. In addition, the preprocessing circuit has current sensing and low pass filter, which can be designed to obtain 2 kHz cut-off frequency.

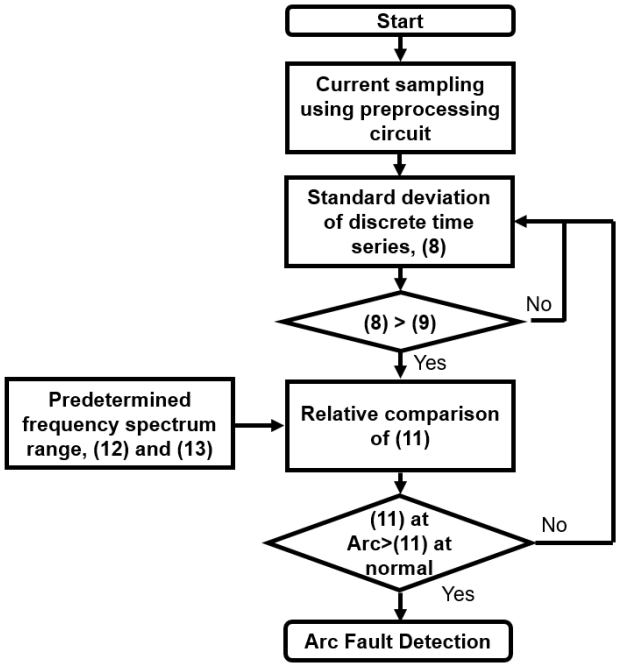

FIGURE 8. Detection algorithm for arc fault condition.

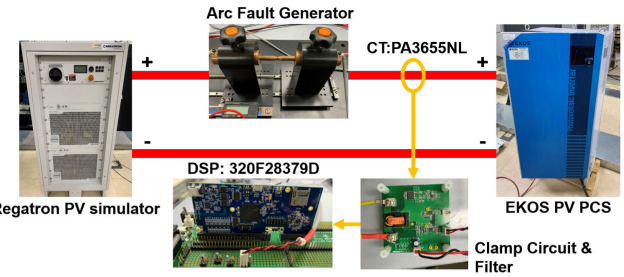

FIGURE 9. Arc fault detection experimental setup.

Fig. 8 presents the proposed arc fault detection algorithm. The preprocessing circuit which including the current sensor and low pass filter measures the DC current. In terms of time domain, the standard deviation using (8) can be calculated to detect the abnormal current variation. When (8) is over the threshold value of (9), the standard deviation of FFT results are relatively compared between normal and abnormal conditions. The frequency range of relative comparison is predetermined with (12) and (13). When (11) at the abnormal condition is higher than the (11) at the normal condition, the arc fault condition is detected. Using the proposed algorithm, the inverter's step load change and turn's on and off can satisfy (8) > (9) condition. However, these operations cannot pass the relative comparison of standard deviation using (11). Therefore, the proposed algorithm can detect the arc fault condition with overcoming the switching noise of inverter. Also, it can distinguish the arc fault condition and other inverter's operation.

IV. EXPERIMENTAL RESULTS

The experimental setup for arc fault detection is designed according to the UL1699B standard, as illustrated in Fig. 9.

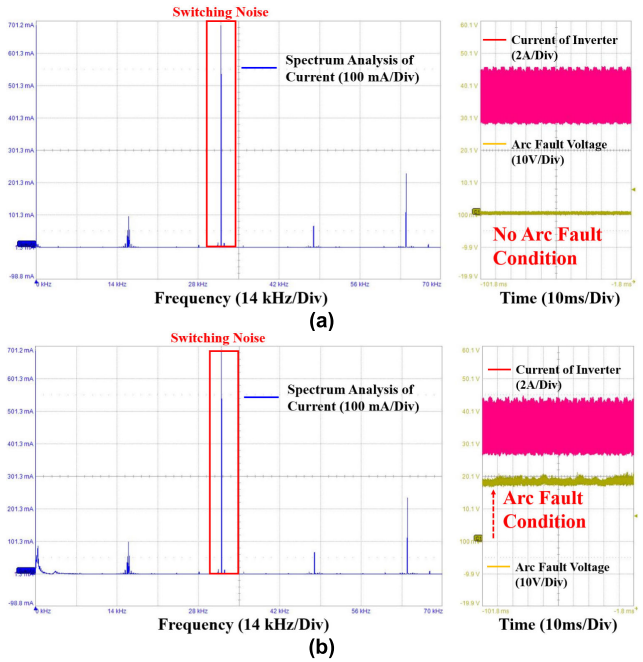

FIGURE 10. Frequency analysis (0 Hz to 70 kHz) of inverter current: (a) no arc condition, and (b) arc fault condition.

The arc fault generator and decoupling circuit are used to follow the experimental setup standard of UL1699B. The decoupling circuit works as line and PV array impedances. It is small impedance value, which is not significant at the low frequency resonance at the arc fault condition. The power source (TC.P.32.1000.400.S, REGATRON) simulates the PV panels. The PV inverter is a commercial product (sample 1).

The DSP controller (TMS320F28379D, TI) implements the arc fault detection algorithm.

Fig. 10 shows the frequency spectrum of the inverter current according to the arc and no arc conditions. Several tens kilo-hertz has a high switching noise by the grid-connected inverter. Therefore, the investigation of arc fault condition in this frequency spectrum is hard to detect the fault condition, which induces poor detection precision. Fig. 2 shows the frequency spectrum of the inverter current at a designed low frequency range according to the arc and no arc fault conditions. It shows the significant magnitude variation between two cases. In addition, this frequency range can avoid the switching noise of inverter. Therefore, the designed frequency range is proper for detecting the arc fault condition.

Fig. 11 shows the experimental verification of arc fault detection performance. Fig. 11 (a) shows the steady state operation of grid-connected inverter at the no arc fault condition, which shows no arc voltage at the arc fault generator. Fig. 11 (b) shows the arc fault detection at the rated load condition. When the arc fault occurs, the arc fault generator induces the voltage drop and current fluctuation. The proposed algorithm implements the time domain and frequency domain analysis, which requires the 81.92 ms computation time under the designed condition. This detection speed can

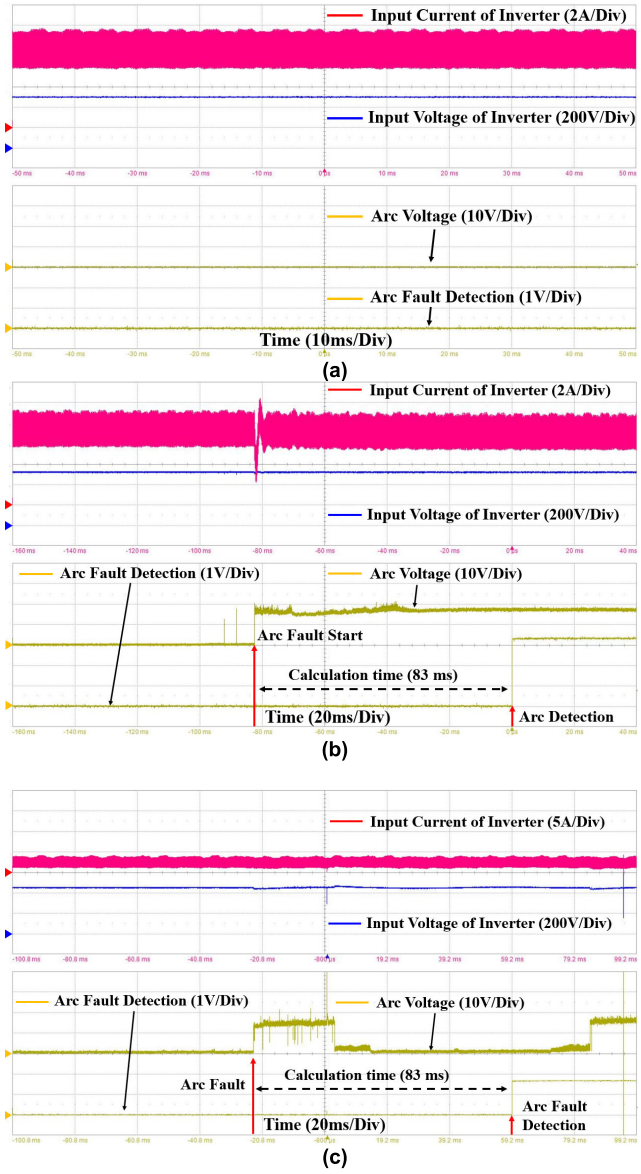

FIGURE 11. Experimental results: (a) normal operation, (b) arc fault condition at 3.5 kW condition, and (c) arc fault condition at 1 kW light load condition.

satisfy the UL 1699B standard (2.5 s). Fig. 11 (c) shows the small energy arc fault detection at the light load condition. The energy of arc fault condition can be calculated as 1.125 J for 81.92 ms.

Fig. 12 shows the transient operation of grid-connected inverter. Fig. 12 (a) presents operational waveform of inverter's turn-on condition, which shows the PV input current gradually increase under the soft-start duration. Fig. 12 (b) presents the operational waveform of inverter's turn-off condition, which shows the drastic current drop. Fig. 12 (c) presents the step load response of inverter, which shows the PV input current change according to the irradiation of PV. The proposed algorithm can distinguish the arc fault condition and other inverter's operation.

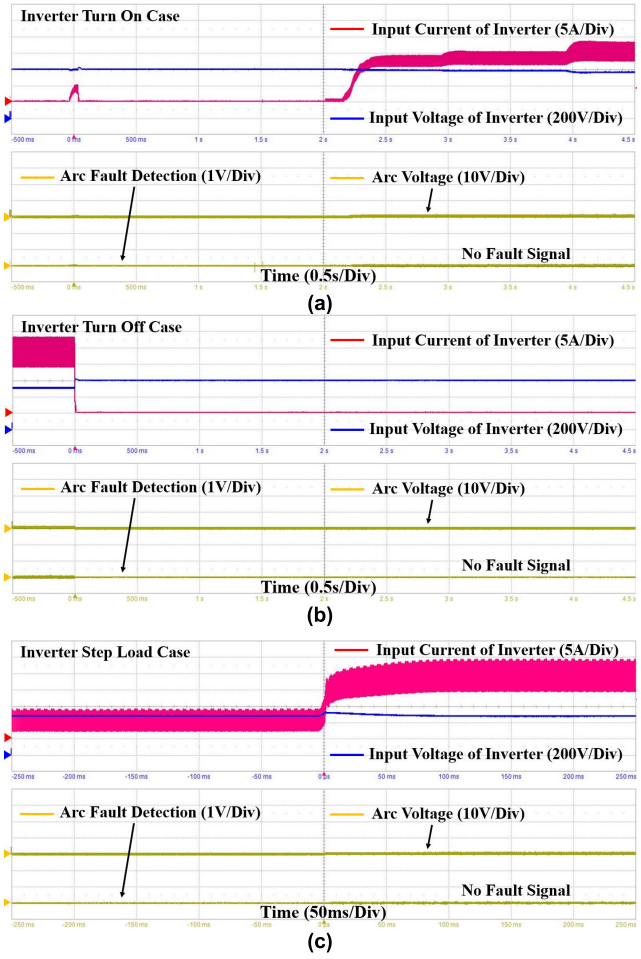

FIGURE 12. Arc fault detection performance: (a) turn on case of the inverter, (b) turn off case of the inverter, and (c) step load response.

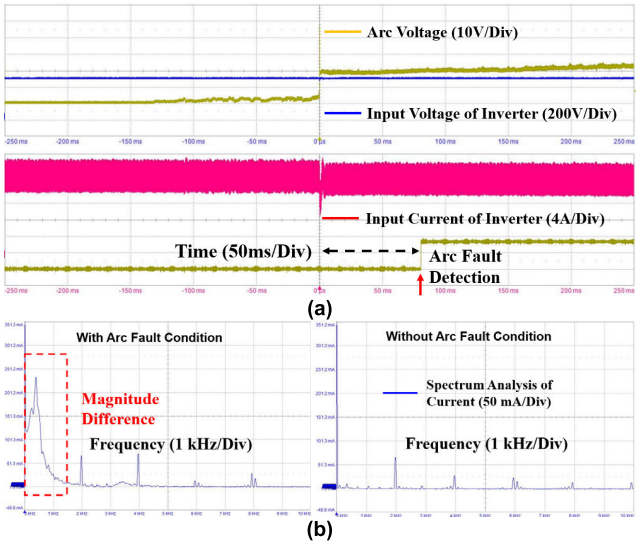

FIGURE 13. Arc fault detection performance: (a) Arc fault condition at 5 kW condition, and (b) frequency spectrum analysis.

Fig. 13 presents the repetitive experimental results to verify the reliability of proposed algorithm and performance of arc fault detection using other brand PV inverter (sample 2). The proposed algorithm can detect the arc fault condition, as shown in Fig. 13 (a). In addition, the frequency spectrum analysis of input current shows the large magnitude difference at the low frequency range, as shown in Fig. 13 (b).

V. CONCLUSION

In this paper, the arc fault detection algorithm is proposed with employing the time series and frequency spectrum analysis. The proposed algorithm detects the steep variation of standard deviation of time series, which can sense the variation of current according to the arc fault. After the time domain detection, the standard deviation of FFT magnitude is relatively compared with the normal and abnormal conditions. The frequency range of relative comparison can be designed with the impedance of arc fault condition, which is investigated with the small signal modeling. The designed frequency range can increase arc fault detection precision with overcoming the switching noise of inverter. The proposed algorithm is verified with the experimental results of 3.5 kW test-bed system. The designed algorithm can distinguish between arc fault condition and other inverter's operation. In addition, it can detect 1.125 J small energies under light load condition. The arc fault can be detected within 90 ms, which can satisfy the UL 1699B standard.

REFERENCES

[1] J. M. Carrasco, L. G. Franquelo, J. T. Bialasiewicz, E. Galvan, R. C. PortilloGuisado, M. A. M. Prats, J. I. Leon, and N. Moreno-Alfonso, "Power-electronic systems for the grid integration of renewable energy sources: A survey," *IEEE Trans. Ind. Electron.*, vol. 53, no. 4, pp. 1002–1016, Jun. 2006.

[2] F. Blaabjerg, Z. Chen, and S. B. Kjaer, "Power electronics as efficient interface in dispersed power generation systems," *IEEE Trans. Power Electron.*, vol. 19, no. 5, pp. 1184–1194, Sep. 2004.

[3] M. A. Mansor, K. Hasan, M. M. Othman, S. Z. B. M. Noor, and I. Musirin, "Construction and performance investigation of three-phase solar PV and battery energy storage system integrated UPQC," *IEEE Access*, vol. 8, pp. 103511–103538, 2020.

[4] M. Faisal, M. A. Hannan, P. J. Ker, A. Hussain, M. B. Mansor, and F. Blaabjerg, "Review of energy storage system technologies in microgrid applications: Issues and challenges," *IEEE Access*, vol. 6, pp. 35143–35164, 2018.

[5] H. Shin and J. H. Roh, "Framework for sizing of energy storage system supplementing photovoltaic generation in consideration of battery degradation," *IEEE Access*, vol. 8, pp. 60246–60258, 2020.

[6] J.-Y. Kim, J.-H. Jeon, S.-K. Kim, C. Cho, J. Ho Park, H.-M. Kim, and K.-Y. Nam, "Cooperative control strategy of energy storage system and microsources for stabilizing the microgrid during islanded operation," *IEEE Trans. Power Electron.*, vol. 25, no. 12, pp. 3037–3048, Dec. 2010.

[7] F. Blaabjerg, R. Teodorescu, M. Liserre, and A. V. Timbus, "Overview of control and grid synchronization for distributed power generation systems," *IEEE Trans. Ind. Electron.*, vol. 53, no. 5, pp. 1398–1409, Oct. 2006.

[8] N. Hatziargyriou, H. Asano, R. Iravani, and C. Marnay, "Microgrids," *IEEE Power Energy Mag.*, vol. 5, no. 4, pp. 78–94, Jul./Aug. 2007.

[9] J. Shen, C. Jiang, Y. Liu, and X. Wang, "A microgrid energy management system and risk management under an electricity market environment," *IEEE Access*, vol. 4, pp. 2349–2356, 2016.

[10] N. L. Georgijevic, M. V. Jankovic, S. Srdic, and Z. Radakovic, "The detection of series arc fault in photovoltaic systems based on the arc current entropy," *IEEE Trans. Power Electron.*, vol. 31, no. 8, pp. 5917–5930, Aug. 2016.

[11] Q. Xiong, X. Feng, A. L. Gattozzi, X. Liu, L. Zheng, L. Zhu, S. Ji, and R. E. Hebner, "Series arc fault detection and localization in DC distribution system," *IEEE Trans. Instrum. Meas.*, vol. 69, no. 1, pp. 122–134, Jan. 2020.
[12] M. Naidu, T. J. Schoepf, and S. Gopalakrishnan, "Arc fault detection scheme for 42-V automotive DC networks using current shunt," *IEEE Trans. Power Electron.*, vol. 21, no. 3, pp. 633–639, May 2006.
[13] W. Kwon, S. Choi, C. Ban, S. Bang, C. Kim, and G. Choe, "A study on the effect of arc fault on switched-mode power supply," in *Proc. 8th Int. Conf. Power Electron. (ECCE Asia)*, Jeju, South Korea, May/Jun. 2011, pp. 3029–3032.
[14] M. K. Alam, F. Khan, J. Johnson, and J. Flicker, "A comprehensive review of catastrophic faults in PV arrays: Types, detection, and mitigation techniques," *IEEE J. Photovolt.*, vol. 5, no. 3, pp. 982–997, May 2015.
[15] Q. Lu, Z. Ye, M. Su, Y. Li, Y. Sun, and H. Huang, "A DC series arc fault detection method using line current and supply voltage," *IEEE Access*, vol. 8, pp. 10134–10146, 2020.
[16] G. Bao, R. Jiang, and X. Gao, "Novel series arc fault detector using high-frequency coupling analysis and multi-indicator algorithm," *IEEE Access*, vol. 7, pp. 92161–92170, 2019.
[17] S. Chae, J. Park, and S. Oh, "Series DC arc fault detection algorithm for DC microgrids using relative magnitude comparison," *IEEE J. Emerg. Sel. Topics Power Electron.*, vol. 4, no. 4, pp. 1270–1278, Dec. 2016.
[18] S. Chen, X. Li, and J. Xiong, "Series arc fault identification for photovoltaic system based on time-domain and Time-Frequency-Domain analysis," *IEEE J. Photovolt.*, vol. 7, no. 4, pp. 1105–1114, Jul. 2017.
[19] Z. Wang and R. S. Balog, "Arc fault and flash signal analysis in DC distribution systems using wavelet transformation," *IEEE Trans. Smart Grid*, vol. 6, no. 4, pp. 1955–1963, Jul. 2015.
[20] X. Yao, L. Herrera, S. Ji, K. Zou, and J. Wang, "Characteristic study and time-domain Discrete- wavelet-transform based hybrid detection of series DC arc faults," *IEEE Trans. Power Electron.*, vol. 29, no. 6, pp. 3103–3115, Jun. 2014.
[21] S. Lu, T. Sirojan, B. T. Phung, D. Zhang, and E. Ambikairajah, "DA-DCGAN: An effective methodology for DC series arc fault diagnosis in photovoltaic systems," *IEEE Access*, vol. 7, pp. 45831–45840, 2019.
[22] N. Qu, J. Zuo, J. Chen, and Z. Li, "Series arc fault detection of indoor power distribution system based on LVQ-NN and PSO-SVM," *IEEE Access*, vol. 7, pp. 184020–184028, 2019.
[23] J. Jiang, Z. Wen, M. Zhao, Y. Bie, C. Li, M. Tan, and C. Zhang, "Series arc detection and complex load recognition based on principal component analysis and support vector machine," *IEEE Access*, vol. 7, pp. 47221–47229, 2019.
[24] B. Hao, "AI in arcing-HIF detection: A brief review," *IET Smart Grid*, vol. 3, no. 4, pp. 435–444, Aug. 2020.
[25] M. Streck, F. Nothnagel, and F. Berger, "Parameters' values of small signal equivalent circuit of electric arc gaps in DC networks," in *Proc. 50th Int. Universities Power Eng. Conf. (UPEC)*, Sep. 2015, pp. 1–6.

HWA-PYEONG PARK (Member, IEEE) was born in Gimcheon, South Korea, in 1991. He received the Ph.D. degree in electrical engineering from the Ulsan National Institute of Science and Technology (UNIST), Ulsan, South Korea, in 2019. He is currently working with the Energy Efficiency Division, Korea Institute of Energy Research (KIER). His main research interests include high-power-density dc–dc converters, power control algorithm for power converters, and battery management systems.

SUYONG CHAE (Member, IEEE) received the B.S. and M.S. degrees in electrical engineering from the Korea Advanced Institute of Science and Technology, Daejeon, South Korea, in 1998 and 2000, respectively, and the Ph.D. degree in electrical engineering from Seoul National University, Seoul, South Korea, in 2009. From 2000 to 2010, he was a Research Engineer with Samsung SDI. Since 2010, he has been a Principle Researcher with the Korea Institute of Energy Research (KIER), Daejeon. His current research interests include power electronics, modeling, and control of distributed power systems.